DESY 09-083
TUM-HEP 724/09

Decaying Dark Matter in Light of the PAMELA and Fermi LAT Data

Alejandro Ibarra* and David Tran†

Physik-Department T30d, Technische Universität München,

James-Franck-Straße, 85748 Garching, Germany.

Christoph Weniger‡

Deutsches Elektronen-Synchrotron DESY,

Notkestraße 85, 22607 Hamburg, Germany.

Abstract

A series of experiments measuring high-energy cosmic rays have recently reported strong indications for the existence of an excess of high-energy electrons and positrons. If interpreted in terms of the decay of dark matter particles, the PAMELA measurements of the positron fraction and the Fermi LAT measurements of the total electron-plus-positron flux restrict the possible decaying dark matter scenarios to a few cases. Analyzing different decay channels in a model-independent manner, and adopting a conventional diffusive reacceleration model for the background fluxes of electrons and positrons, we identify some promising scenarios of dark matter decay and calculate the predictions for the diffuse extragalactic gamma-ray flux, including the contributions from inverse Compton scattering with the interstellar radiation field.

*Electronic address: alejandro.ibarra@ph.tum.de

†Electronic address: david.tran@ph.tum.de

‡Electronic address: christoph.weniger@desy.de

I. INTRODUCTION

Different experiments measuring high-energy cosmic rays have over the last months reported a wealth of new results pointing to the existence of an exotic source of electrons and positrons. The PAMELA collaboration reported evidence for a sharp rise of the positron fraction at energies $7 - 100$ GeV [1], possibly extending toward even higher energies, compared to the expectations from spallation of primary cosmic rays on the interstellar medium [2]. This result confirmed previous hints about the existence of a positron excess from HEAT [3], CAPRICE [4] and AMS-01 [5]. Almost at the same time, the balloon-borne experiments ATIC [6] and PPB-BETS [7] reported the discovery of a peak in the total electron-plus-positron flux at energies $600 - 700$ GeV, while the H.E.S.S. collaboration [8] reported a substantial steepening in the high-energy electron-plus-positron spectrum above 600 GeV compared to lower energies.

These results raised a lot of interest in the astrophysics and particle physics communities, leading to many proposals trying to explain this excess. One of the most popular astrophysical interpretations of the positron excess is in terms of the electron-positron pairs produced by the interactions of high-energy photons in the strong magnetic field of pulsars [9, 10, 11]. However, this interpretation requires a rather large fraction of the spin-down power being injected in the form of electron-positron pairs or a rather large rate of gamma-ray pulsar formation. Alternatively, the positrons could be originating from the decay of charged pions, which are in turn produced by the hadronic interactions of high-energy protons accelerated by nearby sources [12].

An arguably more exciting explanation of the cosmic-ray positron excess is the possibility that the positrons are produced in the annihilation or the decay of dark matter particles. Should this interpretation be confirmed by future experiments, then the positron excess would constitute the first non-gravitational evidence for the existence of dark matter in our Galaxy. The interpretation of the PAMELA excess in terms of dark matter is subject to constraints from the flux measurements of other cosmic-ray species. A very important constraint arises from the measurements of the antiproton flux by PAMELA [13], BESS95 [14], BESS95/97 [15], CAPRICE94 [16], CAPRICE98 [17] and IMAX [18], which are consistent with the expectations from conventional propagation models, thus excluding the possibility of a large antiproton flux from dark matter annihilation or decay [19, 20].

The steep rise in the positron fraction observed by PAMELA can be explained by dark matter annihilations in the center of the Milky Way, provided the dark matter particle has a mass larger than ~ 150 GeV and annihilates preferentially into leptons of the first or second generation [21]. This interpretation of the positron excess, however, typically requires the *ad hoc* introduction of large boost factors. Furthermore, it has been argued that if dark matter annihilations are the origin of the PAMELA anomaly, then the predicted gamma-ray emission from the center of the Galaxy is in conflict with the H.E.S.S. observations for typical cuspy halo profiles [22]. On the other hand, if the positron excess is due to the decay of dark matter particles, the dark matter particles must have a mass larger than ~ 300 GeV, a lifetime around 10^{26} s, and must decay preferentially into hard leptons of the first or second generation [23]. In this case, no boost factors are required and the gamma and radio measurements are consistent with present measurements [24]. Some recent works on the indirect detection of decaying dark matter can be found in [25, 26, 27, 28].

More recently, the Fermi LAT collaboration has published measurements of the electron-plus-positron flux from 20 GeV to 1 TeV of unprecedented accuracy [29], revealing an energy spectrum that roughly follows a power law $\propto E^{-3.0}$ without any prominent spectral features. Simultaneously, the H.E.S.S. collaboration reported a measurement of the cosmic-ray electron-plus-positron spectrum at energies larger than 340 GeV, confirming the Fermi result of a power-law spectrum with spectral index of $3.0 \pm 0.1(\text{stat.}) \pm 0.3(\text{syst.})$, which furthermore steepens at about 1 TeV [30]. The measured energy spectrum is harder than expected from conventional diffusive models, although it can be accommodated by an appropriate change of the injection spectrum of primary electrons. However, when taken together with the steep rise in the positron fraction as seen by PAMELA up to energies of 100 GeV, the Fermi LAT data suggest the existence of additional Galactic sources of high-energy electrons and positrons with energies up to a few TeV. Furthermore, it should be borne in mind that the determination of the correct Galactic cosmic-ray scenario is still an open problem, and while an electron injection spectrum harder than the conventional could reproduce the Fermi data, it fails to account for the AMS-01 and HEAT data below 20 GeV and the H.E.S.S. data above 1 TeV [31].

In this paper we analyze the constraints that the results of the PAMELA and Fermi collaborations impose on the scenario of decaying dark matter, assuming a GALPROP conventional model as our Galactic cosmic-ray scenario. To this end, we pursue a model-

independent approach, calculating the prediction for the positron fraction and the total electron-plus-positron flux for various decay channels of both a fermionic and a bosonic dark matter particle. We will identify the most promising scenarios in the light of the PAMELA and Fermi data, and we will calculate for those the predictions for the antiproton flux and the diffuse extragalactic gamma-ray flux. Some related works have recently appeared [32, 33].

The paper is organized as follows: in Section 2 we will review the production and propagation in the Galaxy of high-energy electrons/positrons, antiprotons and gamma rays from dark matter decay, including a contribution to the total gamma-ray flux from inverse Compton radiation. In Section 3 we will show the predictions for the positron fraction and the total electron-plus-positron flux for several decaying dark matter scenarios. For the promising scenarios, we will also show the predictions for the antiproton and the gamma-ray fluxes. Finally, in Section 4 we will present our conclusions.

II. COSMIC RAYS

In this section, we briefly review the propagation model for cosmic rays that we need for the calculation of the electron, positron and antiproton fluxes measurable at Earth. Furthermore, we discuss our calculation of the flux of gamma rays, which come from inverse Compton scattering (ICS) with the interstellar radiation field (ISRF) as well as directly from the decay process itself.

If dark matter decays at a sufficiently large rate, the decay products (electrons, positrons, antiprotons and gamma rays) could be observable as an anomalous contribution to the high-energy cosmic-ray fluxes. The production rate of particles per unit energy and unit volume at a position $\vec{r}$ with respect to the center of the Milky Way is given by

$$Q(E,\vec{r}) = \frac{\rho(\vec{r})}{M_{\rm DM}\,\tau_{\rm DM}}\frac{dN}{dE}\ , \tag{1}$$

where dN/dE is the energy spectrum of particles produced in the decay and $\rho(\vec{r})$ is the density profile of dark matter particles in the Milky Way halo. For definiteness we will adopt the spherically symmetric Navarro-Frenk-White halo density profile [34]:

$$\rho(r) = \frac{\rho_0}{(r/r_c)[1+(r/r_c)]^2}\ , \tag{2}$$

with $\rho_0 \simeq 0.26\,{\rm GeV/cm^3}$ and $r_c \simeq 20$ kpc, although our results are almost independent of

choice of the density profile[1].

A. Electron/positron propagation

After being produced in the Milky Way halo, the electrons and positrons propagate through the Galaxy and its diffusive halo in a rather complicated way before reaching the Earth. The propagation is commonly described by a stationary two-zone diffusion model with cylindrical boundary conditions [35]. Under this approximation, the number density of electrons and positrons per unit energy, $f_{e^\pm}(E,\vec{r},t)$, satisfies the following transport equation:

$$0 = \frac{\partial f_{e^\pm}}{\partial t} = \nabla\cdot[K(E,\vec{r})\nabla f_{e^\pm}] + \frac{\partial}{\partial E}[b(E,\vec{r})f_{e^\pm}] + Q_{e^\pm}(E,\vec{r}) \ . \tag{3}$$

The first term on the right-hand side of the transport equation is the diffusion term, which accounts for the propagation through the tangled Galactic magnetic field. The diffusion coefficient $K(E,\vec{r})$ is assumed to be constant throughout the diffusion zone and is parametrized by $K(E) = K_0\ \beta\ \mathcal{R}^\delta$, where $\beta = v/c$ and $\mathcal{R}$ is the rigidity of the particle, which is defined as the momentum in GeV per unit charge, $\mathcal{R} \equiv p(\mathrm{GeV})/Z$. The second term accounts for energy losses due to ICS on starlight or the cosmic microwave background (CMB), synchrotron radiation and ionization. We parameterize the energy loss rate as $b(E) = \frac{E^2}{E_0\tau_E}$, with $E_0 = 1\,\mathrm{GeV}$ and $\tau_E = 10^{26}\,\mathrm{s}$. Lastly, $Q_{e^\pm}(E,\vec{r})$ is the source term of electrons and positrons, defined in Eq. (1).

The boundary conditions for the transport equation, Eq.(3), require the solution $f_{e^\pm}(E,\vec{r},t)$ to vanish at the boundary of the diffusion zone, which is approximated by a cylinder with half-height $L = 1-15$ kpc and radius $R = 20$ kpc. Under these assumptions, the propagation of electrons and positrons can be described by just three parameters, the normalization K_0 and the spectral index δ of the diffusion coefficient, which are related to the properties of the interstellar medium, and the height of the diffusion zone, L. In our numerical analysis we will adopt for these parameters the values of the MED propagation model defined in [36], which provide the best fit to the Boron-to-Carbon (B/C) ratio: $\delta = 0.70$,

[1] Due to the effective energy loss of electrons, the high-energy component of the spectrum mostly originates from sources within the Galactic neighborhood of a few kpc from the Solar System, where the different halo profiles are very similar. We have checked that choosing different halo profiles has a negligible effect on our results (see also [25]).

$K_0 = 0.0112\,\mathrm{kpc}^2/\mathrm{Myr}$ and $L = 4\,\mathrm{kpc}$. Our conclusions, however, are rather insensitive to the choice of propagation parameters, as the different sets of propagation parameters yield rather similar results for cosmic rays from local sources. This is due to the fact that at higher energies above several 10 GeV energy losses dominate the effects of diffusion, rendering the exact propagation model parameters less relevant. We illustrate the dependence of the results on the adopted model parameters for a particular example in Section 3.

The solution of the transport equation at the heliospheric boundary, $r = r_\odot$, $z = 0$, can be formally expressed by the convolution

$$f_{e^\pm}(E) = \frac{1}{M_{\rm DM}\,\tau_{\rm DM}} \int_0^{M_{\rm DM}} dE'\, G_{e^\pm}(E, E')\, \frac{dN_{e^\pm}(E')}{dE'}\,. \tag{4}$$

The Green's function $G_{e^\pm}(E, E')$ encodes all the information about astrophysics (such as the details of the halo profile and the propagation of electrons/positrons in the Galaxy), while the remaining part is model-dependent and is determined by the nature of the dark matter particles. Analytical and numerical expressions for the Green's function for the propagation of electrons/positrons can be found in [25].

Finally, the interstellar flux of primary electrons/positrons from dark matter decay is given by:

$$\Phi^{\rm DM}_{e^\pm}(E) = \frac{c}{4\pi} f_{e^\pm}(E)\,. \tag{5}$$

In order to compare our results with the PAMELA results of the positron fraction as well as the Fermi results on the total flux of electrons plus positrons it is necessary to know the background fluxes of high-energy electrons and positrons. The background flux of positrons is constituted by secondary positrons produced in the collision of primary protons and other nuclei with the interstellar medium. On the other hand, the background flux of electrons is constituted by a primary component, presumably produced in supernova remnants, as well as a secondary component, produced by spallation of cosmic rays on the interstellar medium and which is much smaller than the primary component. Whereas the spectrum of secondary electrons and positrons is calculable in a given propagation model, the energy spectrum and the normalization of the primary electron flux is unknown and has to be determined by direct measurements.

In this paper we will adopt for the background fluxes of electrons and positrons the ones corresponding to the "model 0" presented by the Fermi collaboration in [31], which fits well the low-energy data points of the total electron-plus-positron flux and the positron fraction.

The interstellar background fluxes can be parametrized as:

$$\Phi_{e^-}^{\rm bkg}(E) \;=\; \left(\frac{82.0\,\epsilon^{-0.28}}{1+0.224\,\epsilon^{2.93}}\right)\,{\rm GeV}^{-1}\,{\rm m}^{-2}\,{\rm s}^{-1}\,{\rm sr}^{-1}\;, \tag{6}$$

$$\Phi_{e^+}^{\rm bkg}(E) \;=\; \left(\frac{38.4\,\epsilon^{-4.78}}{1+0.0002\,\epsilon^{5.63}}+24.0\,\epsilon^{-3.41}\right)\,{\rm GeV}^{-1}\,{\rm m}^{-2}\,{\rm s}^{-1}\,{\rm sr}^{-1}\;, \tag{7}$$

where $\epsilon = E/1\,{\rm GeV}$. In the energy regime between 2 GeV and 1 TeV these approximations are better than 5%.

At energies smaller than ~ 10 GeV the electron/positron fluxes at the top of the atmosphere can differ considerably from the interstellar fluxes, due to solar modulation effects. Under the force field approximation [37], the fluxes at the top of the atmosphere are related to the interstellar fluxes by the following simple relation [38]:

$$\Phi_{e^\pm}^{\rm TOA}(E_{\rm TOA}) = \frac{E_{\rm TOA}^2}{E_{\rm IS}^2}\;\Phi_{e^\pm}^{\rm IS}(E_{\rm IS}), \tag{8}$$

where $E_{\rm IS} = E_{\rm TOA} + \phi_F$, with $E_{\rm IS}$ and $E_{\rm TOA}$ being the electron/positron energies at the heliospheric boundary and at the top of the Earth's atmosphere, respectively, and ϕ_F being the solar modulation parameter, which varies between 500 MV and 1.3 GV over the eleven-year solar cycle. In order to compare our predictions with the AMS-01 and HEAT data we will take $\phi_F = 550$ MV [3].

Then, if there exists an exotic source of electrons and positrons from dark matter decay, the total flux of electrons plus positrons and the positron fraction at the top of the atmosphere read, respectively,

$$\Phi^{\rm tot}(E) \;=\; \Phi_{e^-}^{\rm DM}(E) + \Phi_{e^+}^{\rm DM}(E) + k\;\Phi_{e^-}^{\rm bkg}(E) + \Phi_{e^+}^{\rm bkg}(E)\;, \tag{9}$$

$${\rm PF}(E) \;=\; \frac{\Phi_{e^+}^{\rm DM}(E) + \Phi_{e^+}^{\rm bkg}(E)}{\Phi^{\rm tot}(E)}, \tag{10}$$

where we have left the normalization of the primary electron flux as a free parameter, k, to be determined in order to provide a qualitatively good fit to the PAMELA and Fermi measurements.

B. Antiproton propagation

Antiproton propagation in the Galaxy can be described in a similar manner as that of electrons and positrons. However, since antiprotons are much heavier than electrons

Model	δ	K_0 (kpc^2/Myr)	L (kpc)	V_c (km/s)
MIN	0.85	0.0016	1	13.5
MED	0.70	0.0112	4	12
MAX	0.46	0.0765	15	5

TABLE I: Astrophysical parameters compatible with the B/C ratio that yield the minimal (MIN), median (MED) and maximal (MAX) flux of antiprotons.

and positrons, energy losses are negligible. However, antiproton propagation is affected by convection, which accounts for the drift of antiprotons away from the disk induced by the Milky Way's Galactic wind. Following [36] we will assume that it has axial direction and that it is constant inside the diffusion region: $\vec{V}_c(\vec{r}) = V_c \ \mathrm{sign}(z) \ \vec{k}$. Then, the transport equation for antiprotons reads:

$$0 = \frac{\partial f_{\bar{p}}}{\partial t} = \nabla \cdot [K(T,\vec{r}) \nabla f_{\bar{p}} - \vec{V}_c(\vec{r}) f_{\bar{p}}] + Q_{\bar{p}}(T,\vec{r}) \ , \tag{11}$$

where T is the antiproton kinetic energy.

As for the case of electrons and positrons, the solution of the transport equation at the heliospheric boundary, $r = r_\odot$, $z = 0$, can be formally expressed by the convolution

$$f_{\bar{p}}(T) = \frac{1}{M_{\rm DM} \ \tau_{\rm DM}} \int_0^{T_{\rm max}} dT' \ G_{\bar{p}}(T,T') \ \frac{dN_{\bar{p}}(T')}{dT'} \ , \tag{12}$$

where $T_{\rm max} = M_{\rm DM} - m_p$ and m_p is the proton mass. Analytical and numerical expressions for the Green's function $G_{\bar{p}}(T,T')$ can be found in [25]. Finally, the interstellar flux of primary antiprotons from dark matter decay is given by

$$\Phi_{\bar{p}}^{\rm DM}(T) = \frac{v}{4\pi} f_{\bar{p}}(T) \ , \tag{13}$$

where v is the velocity of the antiprotons. The prediction of the antiproton flux from dark matter decay is very sensitive to the choice of propagation parameters. Therefore, we will show the results for three different propagation models that are consistent with the observed B/C ratio and that give the maximal (MAX), median (MED) and minimal (MIN) antiproton flux [36]. The relevant parameters are summarized in Tab. I.

The antiproton flux at Earth is also affected at low energies by solar modulation effects. Again, under the force field approximation [37], the antiproton flux at the top of the Earth's

atmosphere is related to the interstellar antiproton flux [38] by the simple relation:

$$\Phi_{\bar{p}}^{\rm TOA}(T_{\rm TOA}) = \left(\frac{2m_p T_{\rm TOA} + T_{\rm TOA}^2}{2m_p T_{\rm IS} + T_{\rm IS}^2}\right) \Phi_{\bar{p}}^{\rm IS}(T_{\rm IS}), \tag{14}$$

where $T_{\rm IS} = T_{\rm TOA} + \phi_F$, with $T_{\rm IS}$ and $T_{\rm TOA}$ being the antiproton kinetic energies at the heliospheric boundary and at the top of the Earth's atmosphere, respectively.

C. Gamma rays from inverse Compton scattering

As discussed above, electrons and positrons from dark matter decay lose their energy mainly via interaction with the Galactic magnetic field and the ISRF. In the first case (assuming injection energies of the order of 1 TeV) synchrotron radiation in the radio band with frequencies $\mathcal{O}(0.1-100$ GHz) is produced and potentially observable (see *e.g.* Ref. [39]). In the second case, the ICS of electrons and positrons on the ISRF (which includes the cosmic microwave background, thermal dust radiation and starlight) produces gamma rays with energies between 100 MeV and 1 TeV. Recently, ICS in connection with the PAMELA excess was discussed in Refs. [40, 41], and we will follow their treatment. A pedagogical review of ICS can be found in Ref. [42].

The rate of inverse Compton scattering of an electron with energy E_e, where an ISRF photon with an energy between ϵ and $\epsilon + d\epsilon$ is upscattered to energies between E_γ and $E_\gamma + dE_\gamma$, is given by

$$\frac{dN(E_e, \vec{r})}{d\epsilon\, dE_\gamma\, dt} = \frac{3}{4}\frac{\sigma_{\rm T}}{\gamma^2\,\epsilon}\, f_{\rm ISRF}(\epsilon, \vec{r})\, \left[2q\ln q + 1 + q - 2q^2 + \frac{1}{2}\frac{(q\Gamma)^2}{1+q\Gamma}(1-q)\right], \tag{15}$$

where $\sigma_{\rm T} = 0.67$ barn denotes the Compton scattering cross section in the Thomson limit, $\gamma = E_e/m_e$, $q = E_\gamma m_e/(4\epsilon\gamma(m_e\gamma - E_\gamma))$, and $f_{\rm ISRF}(\epsilon, \vec{r})$ denotes the differential number density of ISRF photons with energy ϵ, at spatial position $\vec{r}$.

From Eq. (15) one can derive the energy loss $b_{\rm ICS}(E_e, \vec{r})$ of electrons due to ICS (which represents the dominant contribution to the energy loss rate $b(E_e, \vec{r})$ in the transport equation, Eq. (3)), and the corresponding power $\mathcal{P}(E_\gamma, E_e, \vec{r})$ that is emitted in gamma rays with energies between E_γ and $E_\gamma + dE_\gamma$ via

$$b_{\rm ICS}(E_e, \vec{r}) = \int_0^\infty d\epsilon \int_{\sim\epsilon}^{4\epsilon\gamma^2} dE_\gamma (E_\gamma - \epsilon)\frac{dN(E_e, \vec{r})}{d\epsilon\, dE_\gamma\, dt} \tag{16}$$

and

$$\mathcal{P}(E_\gamma, E_e, \vec{r}) = \int_0^\infty d\epsilon (E_\gamma - \epsilon)\frac{dN(E_e, \vec{r})}{d\epsilon\, dE_\gamma\, dt}. \tag{17}$$

Neglecting diffusion and synchrotron losses[2], the energy distribution of electrons and positrons from dark matter decay it is given by

$$f_{e^\pm}(E_e, \vec{r}) = \frac{1}{b_{\rm ICS}(E_e, \vec{r})} \int_{E_e}^{M_{\rm DM}} d\tilde{E}\, Q_{e^\pm}(\tilde{E}, \vec{r}). \tag{18}$$

For the differential flux of ICS photons of energy E_γ from a region $\Delta\Omega$ of the sky it then follows:

$$\frac{d\Phi}{dE_\gamma} = 2\, \frac{1}{4\pi\, E_\gamma\, \tau_{\rm DM}} \int_{\Delta\Omega} d\Omega \int_{\rm l.o.s.} ds\, \frac{\rho(\vec{r})}{M_{\rm DM}} \int_{m_e}^{M_{\rm DM}} dE_e\, \frac{\mathcal{P}(E_\gamma, E_e, \vec{r})}{b_{\rm ICS}(E_e, \vec{r})}\, Y(E_e), \tag{19}$$

where $Y(E_e) = \int_{E_e}^{M_{\rm DM}} d\tilde{E}\, dN_{e^\pm}/d\tilde{E}$ describes the number of particles in the spectrum of electrons and positrons above a certain energy E_e. In the second integral, the coordinate s runs over the line of sight (l.o.s.), which points in the direction of $\Delta\Omega$. The prefactor 2 takes into account that the same amount of gamma rays comes from the dark matter electrons and positrons. In this work, we use the ISRF data as derived in Ref. [43], and we fully take into account the spatial dependence of the energy loss $b_{\rm ICS}(E_e, \vec{r})$ in Eq. (18). Furthermore, we calculate the gamma rays from ICS with extragalactic origin. In this case, effects of redshifting must also be taken into account. Details of this calculation can be found in Ref. [41].

In addition to the gamma-ray signal from dark matter decay there exists a background contribution, presumably originating from active galactic nuclei (AGN), which is perfectly isotropic, and which has an energy spectrum which is assumed to follow a simple power law; the normalization and index will be treated as free parameters to be determined by requiring a good fit of the total flux to the data.

We will compare our predicted flux to two sets of data for the extragalactic diffuse gamma-ray background obtained from the EGRET data, using two different models for the Galactic background, averaging over the whole sky, excluding the region of the Galactic plane with latitudes $|b| < 10^\circ$. The first analysis of the extragalactic diffuse gamma-ray flux by Sreekumar et al. [44] revealed a power law

$$\left[E^2 \frac{dJ}{dE}\right]_{\rm bkg} = 1.37 \times 10^{-6} \left(\frac{E}{\rm GeV}\right)^{-0.1} ({\rm cm}^2\ {\rm str\ s})^{-1}\ {\rm GeV} \tag{20}$$

[2] In Ref. [32] it was discussed that this approximation gives results for the ICS fluxes that are correct at the $\mathcal{O}(2)$ level, which is sufficient for our analysis.

in the energy range 50 MeV$-$10 GeV. On the other hand, the extraction of the extragalactic background by Strong, Moskalenko and Reimer [45], using an optimized model to better simulate the Galactic diffuse emission, revealed a steeper power law,

$$\left[E^2\frac{dJ}{dE}\right]_{\rm bkg} = 6.8\times10^{-7}\left(\frac{E}{\rm GeV}\right)^{-0.32}\ ({\rm cm}^2\ {\rm str\ s})^{-1}\ {\rm GeV}, \tag{21}$$

between 50 MeV $-$ 2 GeV and an intriguing break of the spectrum at energies 2 GeV $-$ 10 GeV. Future measurements by the Fermi LAT, as well as a better understanding of the Galactic diffuse emission, will provide a better determination of the extragalactic diffuse gamma-ray flux in the near future.

III. PREDICTIONS FROM DECAYING DARK MATTER

We will analyze in this section the predictions for the positron fraction and the total electron-plus-positron flux including a possible contribution from dark matter decay in order to account for the anomalies observed by PAMELA and Fermi. To keep the analysis as model-independent as possible, we will analyze several scenarios of decaying dark matter, computing the predictions for the positron fraction and the total electron-plus-positron flux for either a fermionic or a bosonic particle, which decays into various channels with a branching ratio of 100%. We calculated for each of these channels the energy spectrum of electrons and positrons using the event generator PYTHIA 6.4 [46]. Thus, from the particle physics point of view the only free parameters are the dark matter mass and lifetime. From the astrophysics point of view there are a number of uncertainties, such as the choice of propagation parameters and the choice of the background fluxes of electrons and positrons. As mentioned in the previous section, we will adopt the MED propagation model defined in [36], which provides the best fit to the Boron-to-Carbon (B/C) ratio, although the results are not very sensitive to the particular choice of the propagation model. On the other hand, for the background fluxes of electrons and positrons we will adopt the spectra corresponding to the "model 0" proposed by the Fermi collaboration. However, we will allow for a possible shift in the normalization of the background flux of electrons, which is dominated by primaries, due to our ignorance of the amount of electrons injected in the interstellar medium. In our analysis we will sample several dark matter masses and treat the dark matter lifetime and the normalization of the background flux of electrons as free parameters which will be

determined to provide a qualitatively good fit to the PAMELA and Fermi measurements. Note that below energies of 10 GeV the data is best fitted for normalizations $k \simeq 1$. In our plots, we always used normalization factors $k \geq 0.8$.

Let us now discuss the cases of fermionic and scalar dark matter particles separately.

A. Fermionic dark matter decay

In the case where the dark matter particle is a fermion $\psi_{\rm DM}$, we consider the following decay channels[3]:

$$\begin{aligned} \psi_{\rm DM} &\to Z^0 \nu \,, \\ \psi_{\rm DM} &\to W^{\pm} \ell^{\mp} \,, \\ \psi_{\rm DM} &\to \ell^+ \ell^- \nu \,, \end{aligned} \tag{22}$$

where the three-body decay into charged leptons and a neutrino is assumed to be mediated by the exchange of a scalar particle, motivated by the interesting scenario of a hidden gaugino as dark matter particle [28].

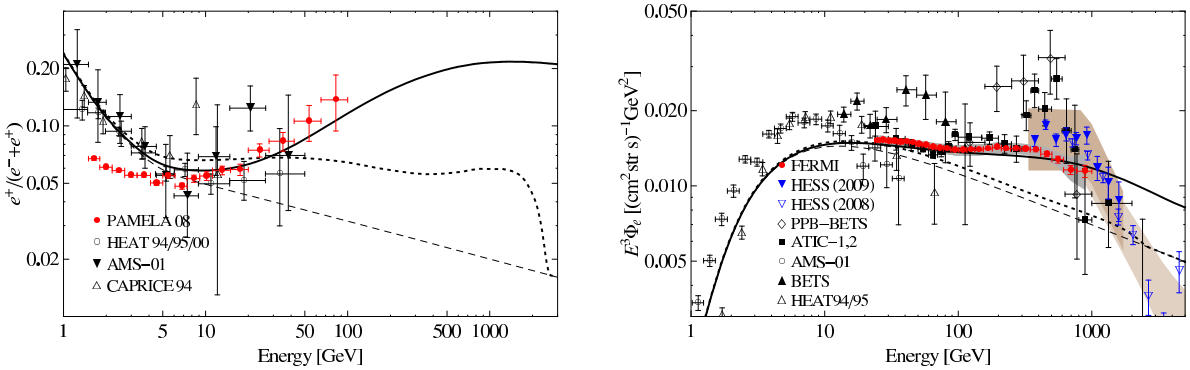

FIG. 1: Positron fraction (*left panel*) and total electron-plus-positron flux (*right panel*) for the decay channel $\psi_{\rm DM} \to Z^0 \nu$ with $M_{\rm DM} = 100\,\text{TeV}$ (solid) and 5 TeV (dotted). The dashed line shows the background fluxes as discussed in the text. Solar modulation is taken into account using the force field approximation with $\phi_F = 550\,\text{MV}$.

The predicted positron fraction in the case where the dark matter particles decay via $\psi_{\rm DM} \to Z^0 \nu$ is shown in the left panel of Fig. 1, compared to the PAMELA, HEAT,

[3] We do not include quarks or Higgs bosons in the list, since they yield similar signatures to gauge boson fragmentation. Furthermore, we only consider decay channels with two or three final-state particles.

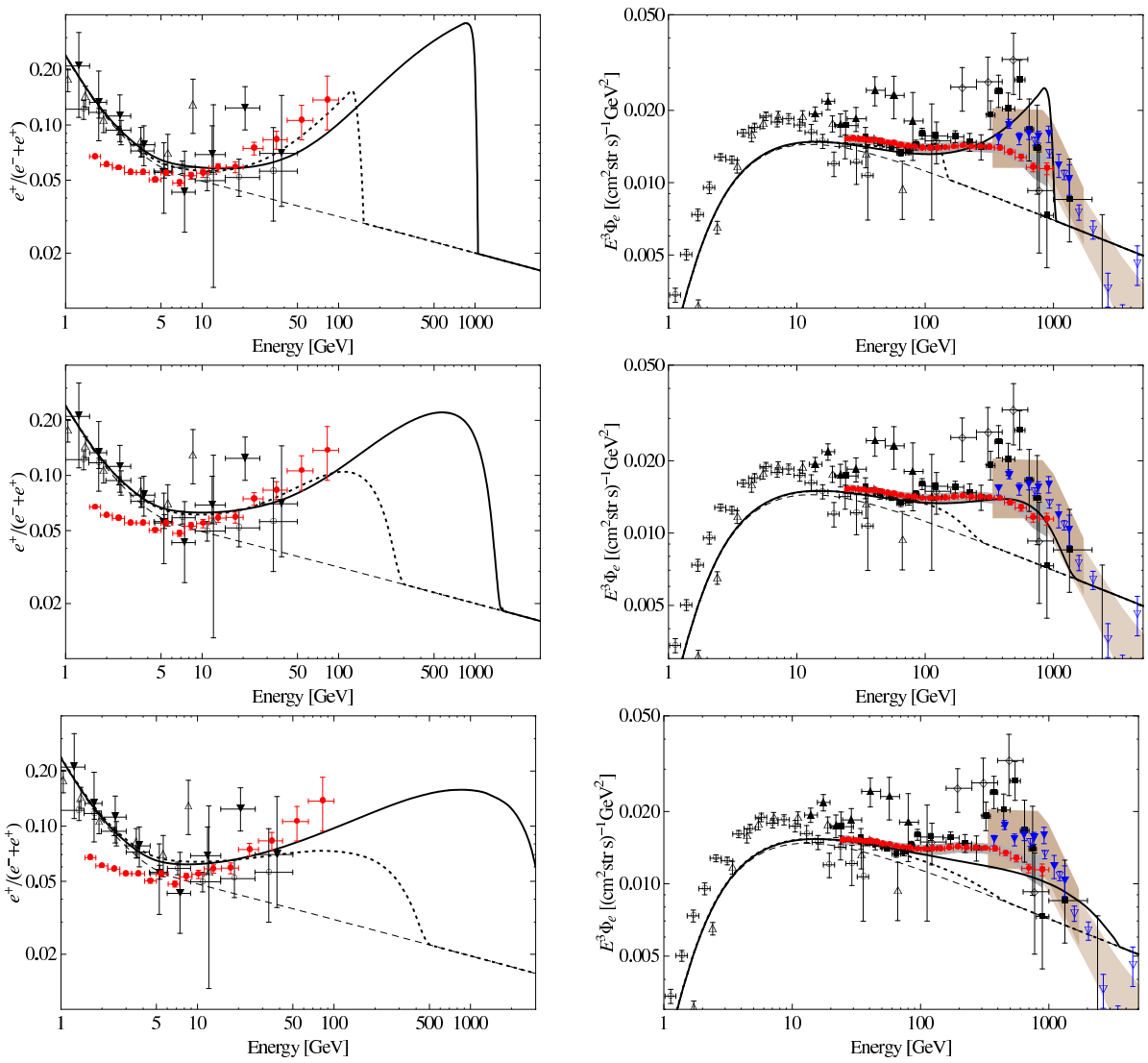

FIG. 2: Same as Fig. 1, but for the decay channels $\psi_{\rm DM} \to W^\pm \ell^\mp$. *Upper panels:* $\psi_{\rm DM} \to W^\pm e^\mp$ with $M_{\rm DM} = 2000\,{\rm GeV}$ (solid) and $300\,{\rm GeV}$ (dotted). *Middle panels:* $\psi_{\rm DM} \to W^\pm \mu^\mp$ with $M_{\rm DM} = 3000\,{\rm GeV}$ (solid) and $600\,{\rm GeV}$ (dotted). *Lower panels:* $\psi_{\rm DM} \to W^\pm \tau^\mp$ with $M_{\rm DM} = 8000\,{\rm GeV}$ (solid) and $1000\,{\rm GeV}$ (dotted).

CAPRICE and AMS-01 data, for the exemplary dark matter masses $M_{\rm DM} = 5$ and 100 TeV. In the right panel we show the corresponding total electron-plus-positron flux compared to the results from Fermi, H.E.S.S., PPB-BETS, BETS, ATIC, HEAT, CAPRICE and AMS-01. The dark matter lifetimes and the normalization factors k of the primary electron flux have been chosen in each case to provide a reasonable fit to the PAMELA and Fermi data points. In this decay channel, the dominant source of electrons and positrons is the fragmentation of the Z^0 boson (with a rather small branching ratio of Z^0 decays into a pair

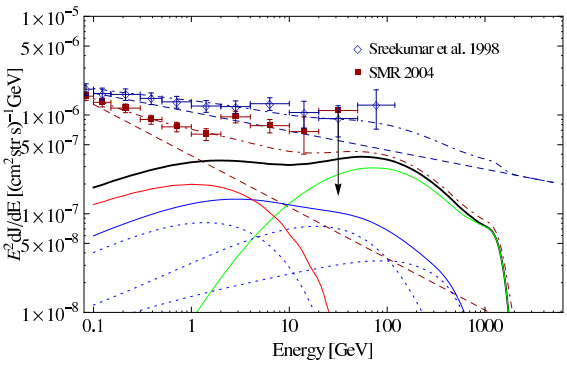

FIG. 3: Extragalactic diffuse gamma-ray flux for $\psi_{\rm DM} \to W^\pm \mu^\mp$ with $M_{\rm DM} = 3000\,{\rm GeV}$ and $\tau_{\rm DM} = 2.1 \times 10^{26}\,{\rm s}$. The gamma-ray flux is averaged over the whole sky, excluding the Galactic plane, $|b| < 10^\circ$. We included gamma rays produced directly in the final-state radiation of the muons and the fragmentation of $W^\pm$ (green line), gamma rays from ICS of dark matter electrons and positrons on the ISRF (solid blue line; the dotted blue lines show, from left to right, the fluxes that come from scattering on the CMB, on the thermal radiation of dust and on starlight) and gamma rays from ICS outside of our Galaxy (red). The black solid line shows the overall flux. The dark red and dark blue lines show the total flux (dash-dotted) adding an isotropic extragalactic background (dashed) with a power-law spectrum. Normalization and power index are chosen to fit one of the two data sets shown [44, 45].

of charged leptons), which produces relatively soft particles. As a result, even though this decay mode can produce a visible excess in the positron fraction, the energy spectrum is in general too flat to explain the steep rise observed by PAMELA. An exception occurs if the dark matter mass is very large, $M_{\rm DM} \gtrsim 50\,{\rm TeV}$. In this case, the electrons and positrons from dark matter decay are boosted to high enough energies to produce the steep rise in the positron fraction. However, these large dark matter masses seem to be in conflict with the H.E.S.S. observations, which require a falloff in the total electron-plus-positron spectrum at $\sim 1\,{\rm TeV}$.

On the other hand, we show in Fig. 2 the predictions for the cosmic-ray electron and positron fluxes when a fermionic dark matter particle decays as $\psi_{\rm DM} \to W^\pm \ell^\mp$ for different dark matter masses. The electrons and positrons created in the fragmentation of the $W^\pm$ gauge bosons produce a rather flat contribution to the positron fraction. However, the hard electrons and positrons resulting from the decay of the $\mu^\pm$ and $\tau^\pm$ leptons or directly from the dark matter decay into $e^\pm$ produce a rise in the total energy spectrum and in the positron

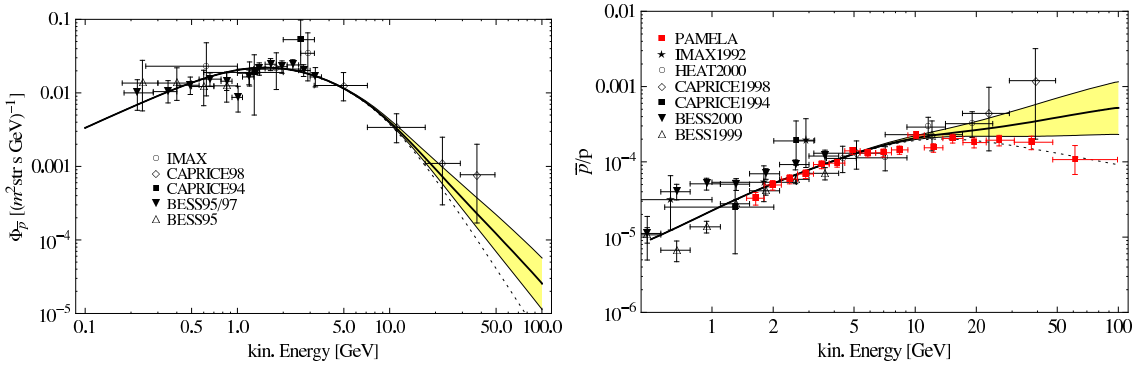

FIG. 4: Antiproton flux (*left panel*) and the corresponding antiproton-to-proton ratio (*right panel*) for $\psi_{\rm DM} \to W^\pm \mu^\mp$ with $M_{\rm DM} = 3000\,{\rm GeV}$ and $\tau_{\rm DM} = 2.1 \times 10^{26}\,{\rm s}$. For the antiproton flux we adopt the background from Ref. [47], while antiproton-to-proton ratio is plotted using the background from Ref. [48], and the yellow band indicates the uncertainties from the propagation model. The solid black line corresponds to the MED model of Tab. I.

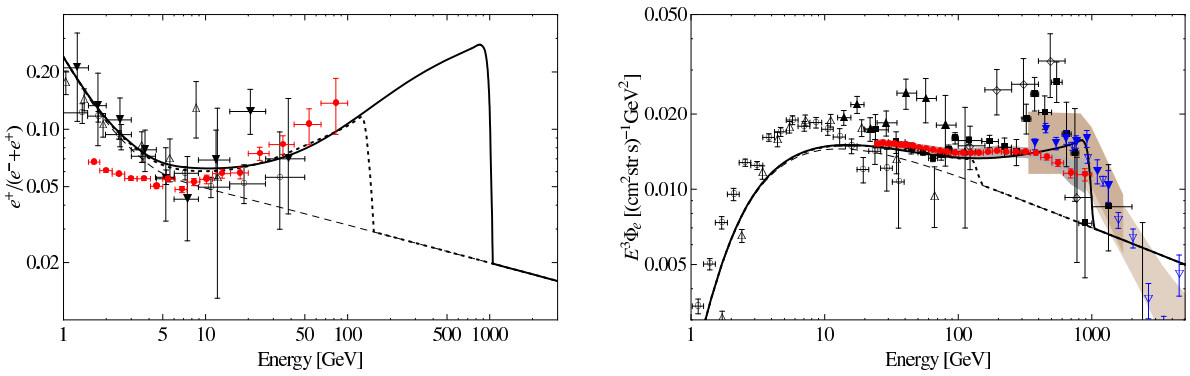

FIG. 5: Same as Fig. 1, but for the flavor-democratic decay $\psi_{\rm DM} \to W^\pm \ell^\mp$ with equal branching ratios into the three charged lepton flavors, for $M_{\rm DM} = 2000\,{\rm GeV}$ (solid) and $300\,{\rm GeV}$ (dotted).

fraction. The decay mode $\psi_{\rm DM} \to W^\pm e^\mp$, which can produce a steep rise in the positron fraction and is thus consistent with the PAMELA observations, produces also a steep rise and a sharp falloff in the total electron-plus-positron flux, which is not observed by Fermi. Thus, the possibility that the dark matter particles decay preferentially in this decay mode, which is well compatible the PAMELA observations, is now strongly disfavored by the Fermi results on the total electron-plus-positron flux.

The decay mode $\psi_{\rm DM} \to W^\pm \mu^\mp$, however, can nicely accommodate the PAMELA and Fermi observations when the dark matter mass is $M_{\rm DM} \simeq 3\,{\rm TeV}$ and the lifetime is $\tau_{\rm DM} \simeq 2.1 \times 10^{26}\,{\rm s}$. In this decay mode, the fragmentation of the $W^\pm$ gauge bosons also produces fluxes of primary antiprotons and gamma rays, which are severely constrained by present

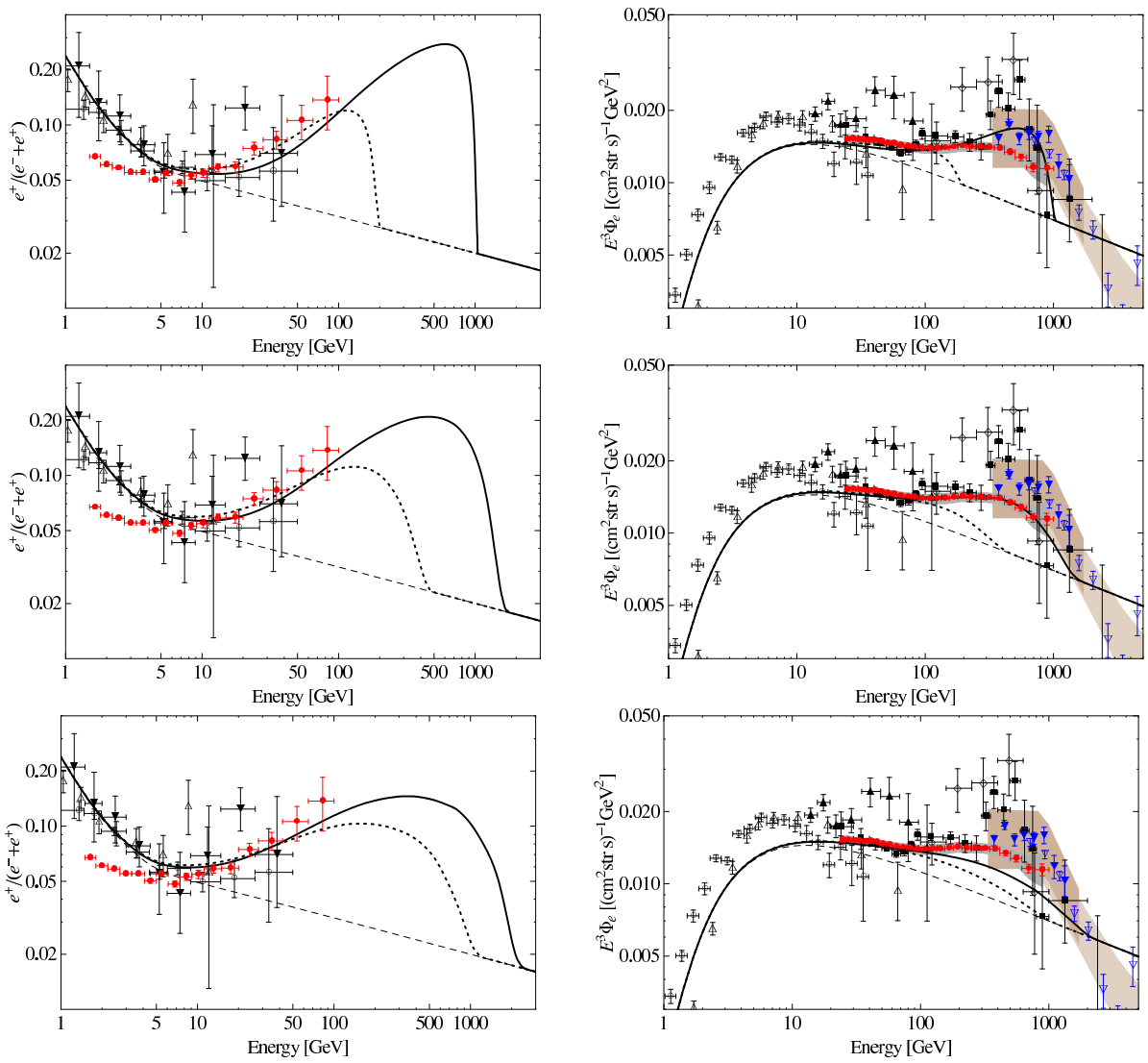

FIG. 6: Same as Fig. 1, but for the decay channels $\psi_{\rm DM} \to \ell^\pm \ell^\mp \nu$. *Upper panels:* $\psi_{\rm DM} \to e^- e^+ \nu$ with $M_{\rm DM} = 2000\,{\rm GeV}$ (solid) and 400 GeV (dotted). *Middle panels:* $\psi_{\rm DM} \to \mu^- \mu^+ \nu$ with $M_{\rm DM} = 3500\,{\rm GeV}$ (solid) and 1000 GeV (dotted). *Lower panels:* $\psi_{\rm DM} \to \tau^- \tau^+ \nu$ with $M_{\rm DM} = 5000\,{\rm GeV}$ (solid) and 2500 GeV (dotted).

experiments. The predictions for the gamma-ray and antiproton fluxes for this particular decay mode are shown in Figs. 3 and 4; the former figure shows the gamma-ray fluxes from final-state radiation and $W^\pm$ fragmentation (green), and from Galactic (blue) and extragalactic (red) ICS of dark matter electrons and positrons. We also show the total flux compared to the extraction of the extragalactic diffuse gamma-ray flux by Sreekumar et al. [44] and by Strong, Moskalenko and Reimer [45], averaging over the whole sky excluding the region of the Galactic plane with latitudes $|b| < 10^\circ$ and assuming a power law for

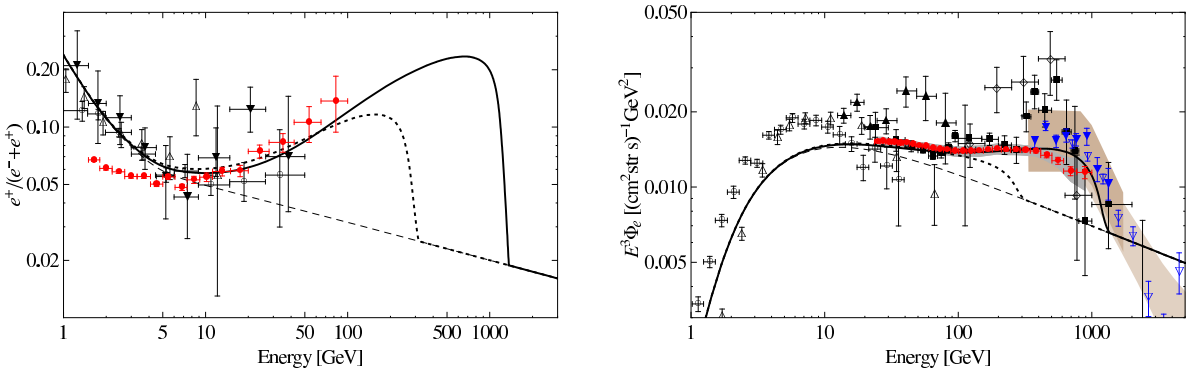

FIG. 7: Same as Fig. 1, but for the democratic decay $\psi_{\rm DM} \to \ell^\pm \ell^\mp \nu$ with equal branching ratios into the three charged lepton flavors, with $M_{\rm DM} = 600\,{\rm GeV}$ (dotted) and $2500\,{\rm GeV}$ (solid).

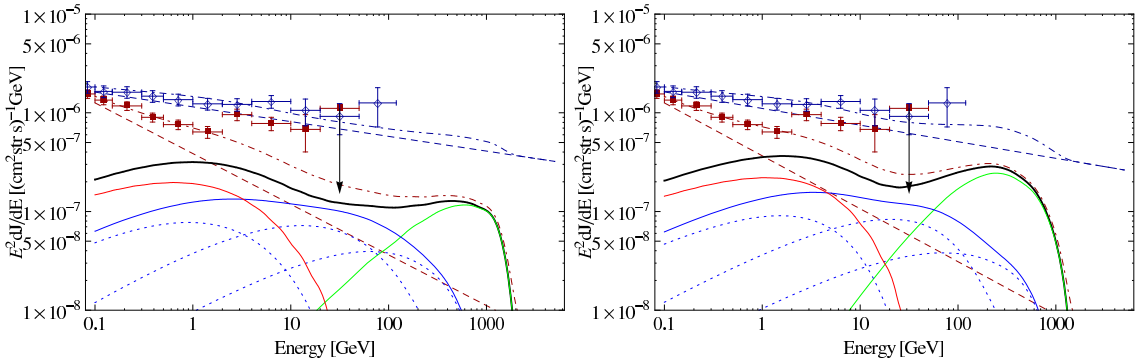

FIG. 8: Same as Fig. 3, but for $\psi_{\rm DM} \to \mu^- \mu^+ \nu$ (*left panel*, with $M_{\rm DM} = 3500\,{\rm GeV}$) and for the democratic decay $\psi_{\rm DM} \to \ell^- \ell^+ \nu$ (*right panel*, with $M_{\rm DM} = 2500\,{\rm GeV}$).

the genuinely extragalactic component. On the other hand, the latter figure shows the prediction for the antiproton-to-proton ratio with an uncertainty band corresponding to the MAX, MED and MIN models in Tab. I. While the absolute flux is compatible with existing measurements, it is apparent from the figure that the antiproton-to-proton ratio is in some tension with the results at the highest energies explored by PAMELA. The fragmentation of the $W^\pm$ gauge bosons also produces a sizable contribution to the total gamma-ray flux at high energies which could be visible by the Fermi LAT as a bump over the background, which is assumed to follow a simple power law, especially if it has a large index as in the extraction of the diffuse extragalactic background from the EGRET data by Strong, Moskalenko and Reimer. Lastly, the decay mode $\psi_{\rm DM} \to W^\pm \tau^\mp$ predicts, for a wide range of dark matter masses, a positron fraction and an electron-plus-positron flux that are too flat to explain the anomalies observed by PAMELA and Fermi.

In some decaying dark matter scenarios, the dark matter particles decay into charged

leptons of different flavors and not exclusively in just one channel. As an illustration of the predictions of this class of scenarios, we show in Fig. 5 the positron fraction and the total electron-plus-positron flux for a dark matter particle that decays democratically into the three flavors, for $M_{\rm DM} = 2000\,{\rm GeV}$ (solid) and 300 GeV (dotted). Although these scenarios could explain the PAMELA excess, the predicted spectral shape of the total flux is not consistent with the Fermi data: either the energy spectrum falls off at too low energies or it presents a sharp peak at high energies, due to the large branching ratio into hard electrons and positrons. Scenarios with smaller branching ratio into electron flavor and larger branching ratio into muon flavor could, however, explain both anomalies simultaneously.

The dark matter particles could also decay into three fermions, namely into a lepton-antilepton pair and a neutrino. In this case many possibilities could arise depending on the specific particle physics scenario. We will just concentrate on the case where the lepton and the antilepton carry the same flavor and the decay is mediated by a heavy scalar[4]. The results for the positron fraction and the total electron-plus-positron flux are shown in Fig. 6.

The spectrum produced in the decay into electron-positron pairs is flatter in this case than in the two-body decay $\psi_{\rm DM} \to W^{\pm} e^{\mp}$, although it still predicts a rather prominent bump in the electron spectrum at high energies, which is not observed by Fermi. More promising is the decay channel $\psi_{\rm DM} \to \mu^- \mu^+ \nu$, which can reproduce quite nicely the Fermi electron-plus-positron spectrum and the steep rise in the positron fraction observed by PAMELA when the dark matter mass is $M_{\rm DM} \simeq 3500\,{\rm GeV}$ and the lifetime is $\tau_{\rm DM} \simeq 1.1 \times 10^{26}\,{\rm s}$. Lastly, decays into tau flavor can qualitatively reproduce the steep rise in the positron fraction for dark matter masses above $\sim 2.5\,{\rm TeV}$, although as apparent from Fig. 6, lower right panel, the resulting electron-plus-positron spectrum has an energy dependence much steeper than $E^{-3.0}$ at high energies, in tension with the Fermi measurements. In this case an additional source of high-energy positrons, coming *e.g.* from pulsars, must be invoked in order to reproduce the Fermi energy spectrum.

As for the two-body decays $\psi_{\rm DM} \to W^{\pm} \ell^{\mp}$, the dark matter particle could also decay into charged fermions with different flavor. We illustrate such a situation showing in Fig. 7 the predictions for the positron fraction and the total electron-plus-positron flux when the dark matter particles decay democratically into the three flavors, for dark matter masses

[4] Our results are not very sensitive to the mass splitting between dark matter particle and virtual scalar.

$M_{\rm DM} = 600\,{\rm GeV}$ (dotted) and $2500\,{\rm GeV}$ (solid). In particular, this is the case in scenarios where dark matter neutralinos decay into light hidden gauginos via kinetic mixing, or vice versa [28]. It is interesting that these scenarios can simultaneously explain the PAMELA and Fermi anomalies when the dark matter mass is $M_{\rm DM} \simeq 2500\,{\rm GeV}$. For the two cases of three-body decay into muon flavors and democratic decay, we show the predictions for the extragalactic diffuse gamma-ray fluxes in Fig. 8. In both cases, they are consistent with the present data and show a deviation from the putative power-law behavior of the astrophysical background, which could be observed by the Fermi LAT, depending on the precise spectrum of the genuinely extragalactic contribution to the flux.

We summarize our results for the promising fermionic dark matter scenarios, together with the corresponding dark matter masses and lifetimes, in Tab. II. The impact of choosing other sets of propagation parameters is illustrated in Fig. 9 for the decay mode $\psi_{\rm DM} \to \mu^+\mu^-\nu$.

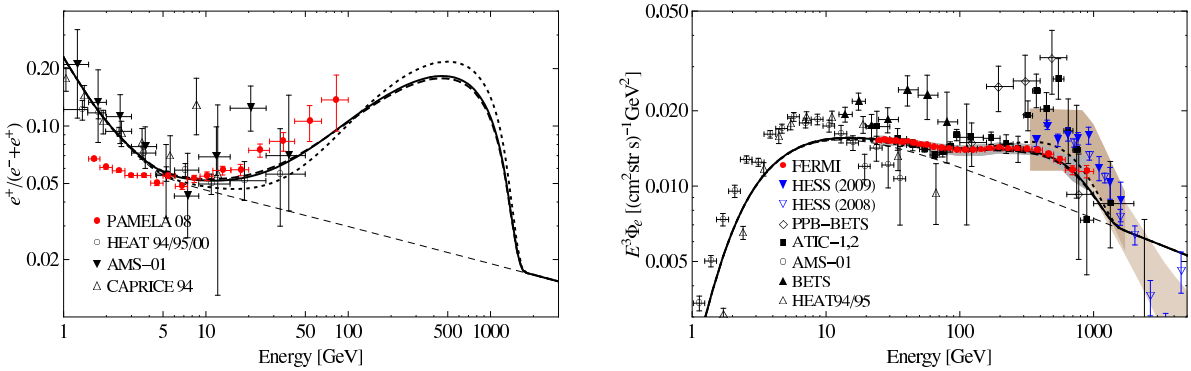

FIG. 9: Illustration of the dependence on the choice of transport parameters. Same as Fig. 6, middle panels, but only for a dark matter mass of 3500 GeV. The solid, dashed and dotted lines correspond to the MED, MAX and MIN model parameters, respectively. The results for the MED and MAX model are very similar because the height of the diffusion zone becomes irrelevant above a few kpc for high-energy electrons from local sources.

B. Scalar dark matter decay

For a scalar dark matter particle, we will discuss the following decay channels[5]:

$$\begin{aligned} \phi_{\rm DM} &\to Z^0 Z^0, \\ \phi_{\rm DM} &\to W^+ W^-, \\ \phi_{\rm DM} &\to \ell^+ \ell^-. \end{aligned} \tag{23}$$

We show in Figs. 10 and 11 the positron fraction and the total electron-plus-positron flux for a scalar dark matter particle that decays exclusively into weak gauge bosons $\phi_{\rm DM} \to Z^0 Z^0$ and $\phi_{\rm DM} \to W^+ W^-$ for dark matter masses $M_{\rm DM} = 2\,{\rm TeV}$ and $10\,{\rm TeV}$. As generically expected from decays into weak gauge bosons, the electrons and positrons produced are relatively soft, resulting in a positron fraction which is too flat to explain the steep rise in the spectrum observed by PAMELA (for an exception with large dark matter masses see Fig. 1).

Decays into harder electrons and positrons can arise in scenarios where the scalar dark matter particle decays into a lepton-antilepton pair. We show in Fig. 12 the predictions for the positron fraction and the total electron-plus-positron flux when the scalar dark matter particle decays into fermions of the same generation, for dark matter masses between $M_{\rm DM} = 300\,{\rm GeV}$ and $5\,{\rm TeV}$. The decay $\phi_{\rm DM} \to e^+ e^-$ can explain the steep rise in the positron fraction observed by PAMELA. However, it is apparent from Fig. 12 that the dark matter decay into this channel cannot be the origin of the Fermi excess in the total electron-plus-positron flux. The situation is similar if one considers democratic decay into all three flavors as shown in Fig. 13. Decays into softer electrons and positrons, as in the case when the dark matter particles decay exclusively via $\phi_{\rm DM} \to \mu^+ \mu^-$, are more promising. In particular, a scalar dark matter particle with a mass $M_{\rm DM} \simeq 2500\,{\rm GeV}$ and a lifetime $\tau_{\rm DM} \simeq 1.8 \times 10^{26}\,{\rm s}$, which decays exclusively into $\mu^+ \mu^-$ pairs, can reproduce both the steep rise in the spectrum observed by PAMELA and the total electron-plus-positron spectrum measured by Fermi. The same holds true for decay into tau flavors, with $M_{\rm DM} \simeq 5000\,{\rm GeV}$ and $\tau_{\rm DM} \simeq 0.9 \times 10^{26}\,{\rm s}$. For these two decay channels, we also show the predictions for the gamma-ray fluxes in Fig. 14, which are again compatible with the present data and present

[5] Again, we do not include quarks or Higgs bosons in the list. Three-body decay modes like $\phi_{\rm DM} \to \ell^+ \ell^- \gamma$ are expected to give results similar to the fermionic dark matter case.

a spectral shape which could be visibly different from a power law, depending on the index of the genuinely extragalactic contribution.

A summary of our results can by found in Tab. II. Note that one of the largest uncertainties that enter in the determination of the dark matter lifetime comes from the determination of the local dark matter density (see Ref. [49] for a recent analysis) since this quantity is inversely proportional to the corresponding flux of cosmic rays.

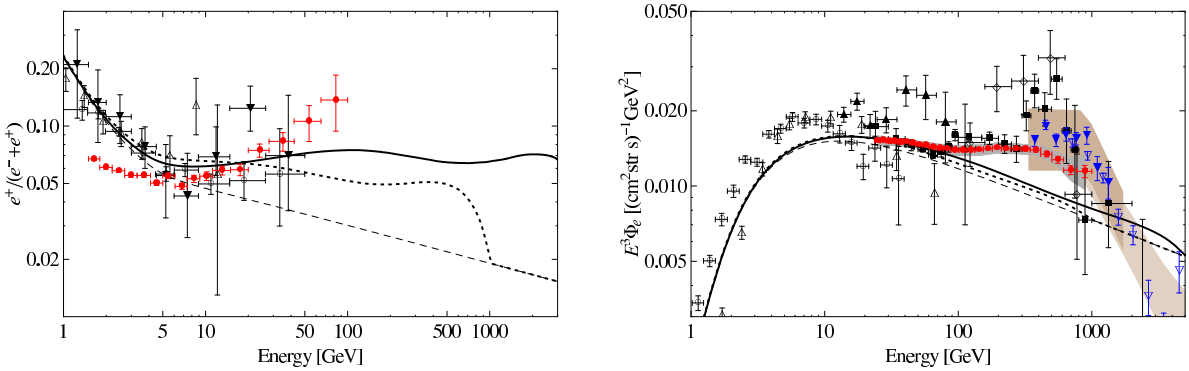

FIG. 10: Same as Fig. 1, but for the decay channel $\phi_{\rm DM} \to Z^0 Z^0$ with $M_{\rm DM} = 10\,{\rm TeV}$ (solid) and 2 TeV (dotted).

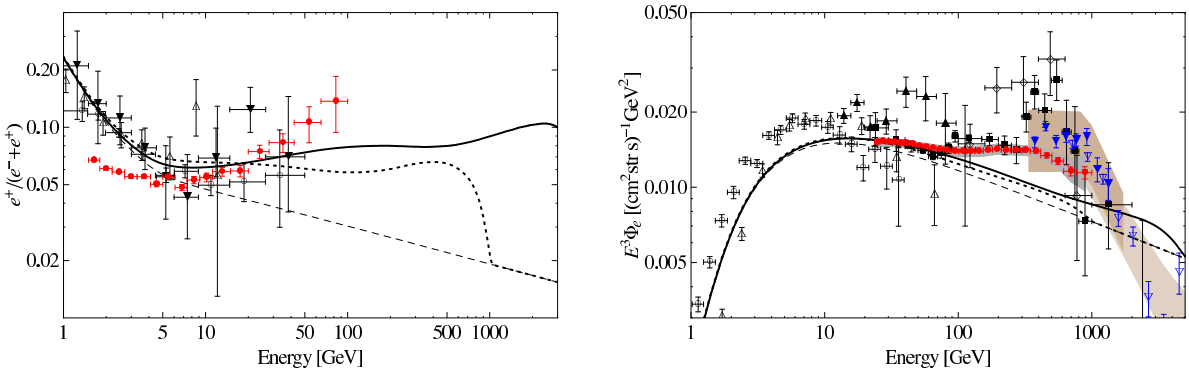

FIG. 11: Same as Fig. 1, but for the decay channel $\phi_{\rm DM} \to W^+ W^-$ with $M_{\rm DM} = 10\,{\rm TeV}$ (solid) and 2 TeV (dotted).

IV. CONCLUSIONS

In some well-motivated dark matter scenarios, the dark matter particles are unstable and decay with a lifetime much longer than the age of the Universe. In this paper we have investigated whether the anomalies in the positron fraction and the total electron-plus-positron flux reported by the PAMELA and the Fermi LAT collaborations, respectively,

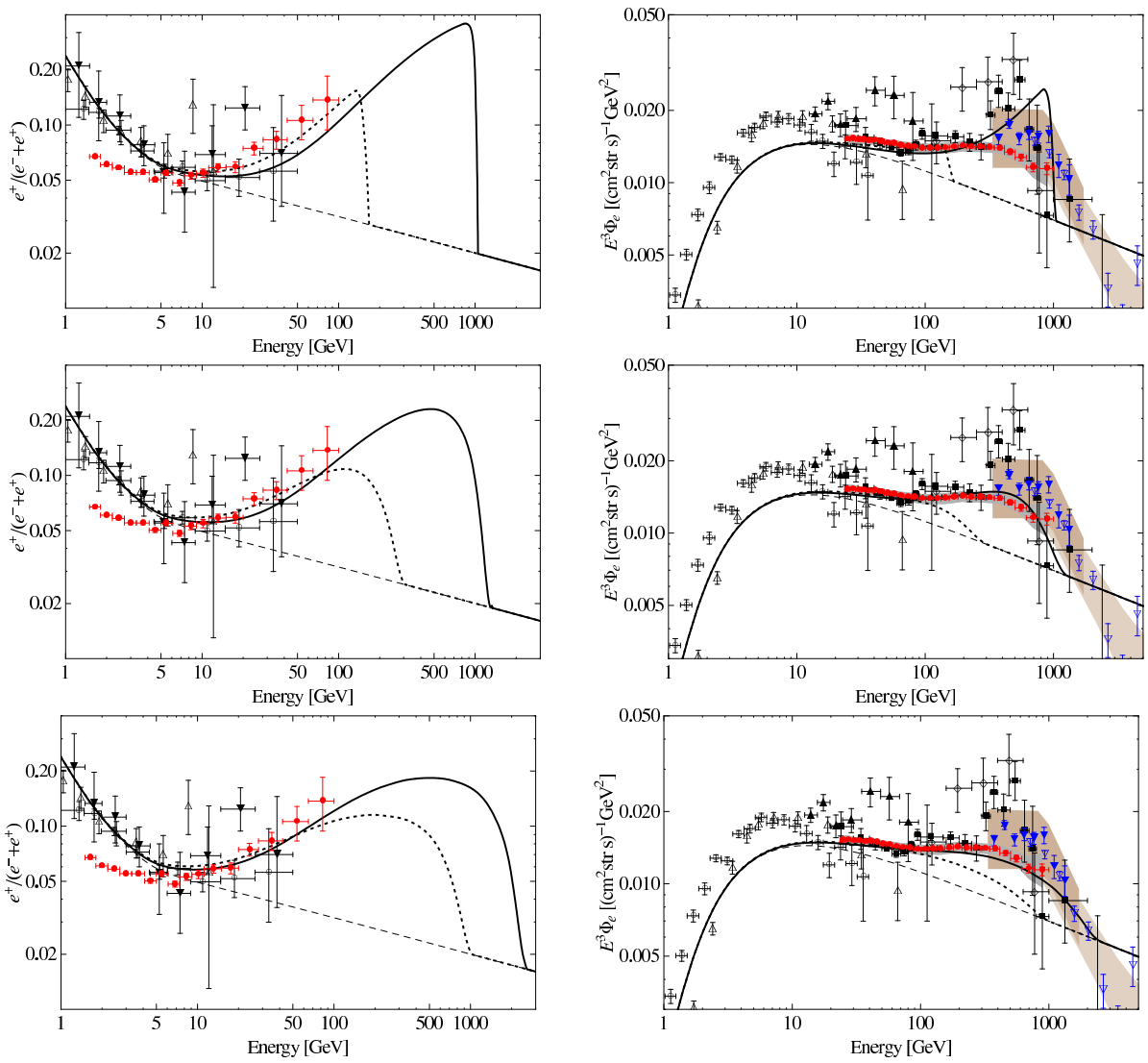

FIG. 12: Same as Fig. 1, but for the decay channels $\phi_{\rm DM} \to \ell^+\ell^-$. *Upper panels:* $\phi_{\rm DM} \to e^+e^-$ with $M_{\rm DM} = 2000\,{\rm GeV}$ (solid) and $300\,{\rm GeV}$ (dotted). *Middle panels:* $\phi_{\rm DM} \to \mu^+\mu^-$ with $M_{\rm DM} = 2500\,{\rm GeV}$ (solid) and $600\,{\rm GeV}$ (dotted). *Lower panels:* $\phi_{\rm DM} \to \tau^+\tau^-$ with $M_{\rm DM} = 5000\,{\rm GeV}$ (solid) and $2000\,{\rm GeV}$ (dotted).

could be interpreted as a signature of the decay of dark matter particles. We have shown that some decaying dark matter scenarios can indeed reproduce the energy spectra of the positron fraction and the total flux reasonably well, while being at the same time consistent with present measurements of the antiproton flux and the diffuse extragalactic gamma-ray flux. The most promising decay channels for a fermionic or a scalar dark matter particle are listed in Tab. II, where we also show the approximate mass and lifetime which provide the best fit to the data. It should be borne in mind that the astrophysical uncertainties in the

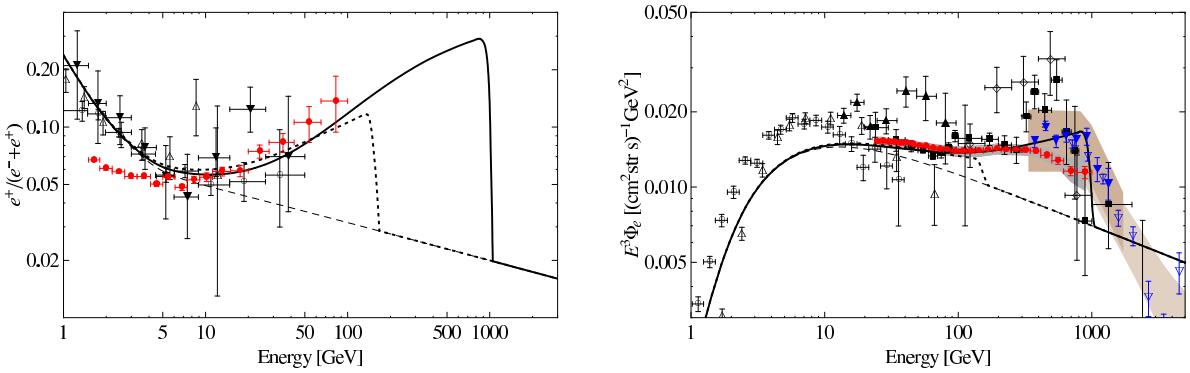

FIG. 13: Same as Fig. 1, but for the decay channel $\phi_{\rm DM} \to \ell^+\ell^-$, democratic decay into three charged lepton flavors, with $M_{\rm DM} = 2000\,{\rm GeV}$ (solid) and $300\,{\rm GeV}$ (dotted).

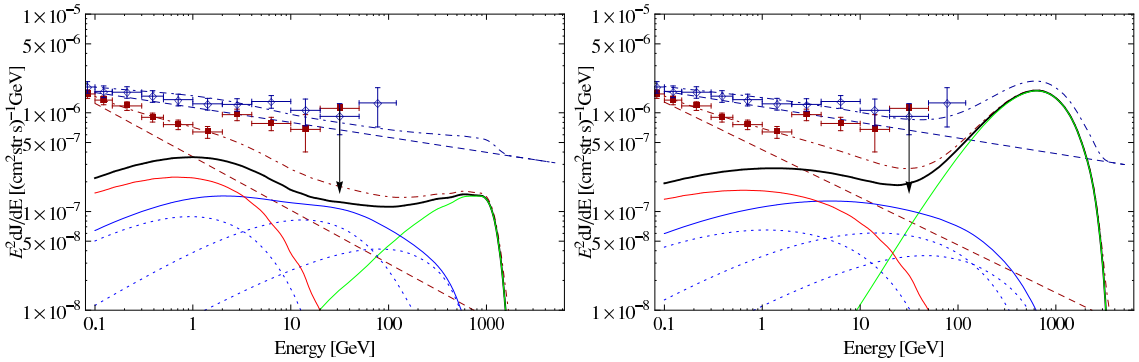

FIG. 14: Same as Fig. 3, but for $\phi_{\rm DM} \to \mu^+\mu^-$ (*left panel*, with $M_{\rm DM} = 2500\,{\rm GeV}$) and $\phi_{\rm DM} \to \tau^+\tau^-$ (*right panel*, with $M_{\rm DM} = 5000\,{\rm GeV}$).

propagation of cosmic rays and in the determination of the background fluxes of electrons and positrons are still large. Besides, the existence of a possibly large primary component of electrons/positrons from astrophysical sources, such as pulsars, cannot be precluded. Therefore, the precise values of the dark matter parameters can vary. The present results can nevertheless be used as a guidance for building models with decaying dark matter as an explanation of the PAMELA and Fermi anomalies.

Future measurements of the extragalactic diffuse gamma-ray flux by the Fermi LAT will provide important information about the decaying dark matter scenario. First, since the Earth is located far from the center of the Milky Way halo, an anisotropy in the diffuse extragalactic gamma-ray flux is expected which could be observed by the Fermi LAT [26]. Moreover, all scenarios in Tab. II predict a departure from a simple power law in the energy spectrum of the extragalactic diffuse background, the deviation depending on the spectrum of the genuinely extragalactic contribution originating presumably from AGN. The observation

Decay Channel	$M_{\rm DM}$ [GeV]	$\tau_{\rm DM}$ [10^{26}s]
$\psi_{\rm DM} \to \mu^+\mu^-\nu$	3500	1.1
$\psi_{\rm DM} \to \ell^+\ell^-\nu$	2500	1.5
$\phi_{\rm DM} \to \mu^+\mu^-$	2500	1.8
$\phi_{\rm DM} \to \tau^+\tau^-$	5000	0.9
$\psi_{\rm DM} \to W^\pm\mu^\mp$	3000	2.1

TABLE II: Decay channels for fermionic and scalar dark matter, $\psi_{\rm DM}$ and $\phi_{\rm DM}$, respectively, that best fit the Fermi and PAMELA data for the MED propagation model and the NFW halo profile. As discussed above, the dependence on the halo profile is negligible, while the dependence on the adopted propagation parameters is illustrated in Fig. 9 for the decay $\psi_{\rm DM} \to \mu^+\mu^-\nu$. The decay mode $\psi_{\rm DM} \to W^\pm\mu^\mp$ is in tension with the PAMELA results on the antiproton-to-proton ratio, as mentioned in the text.

of such a deviation would provide support for the decaying dark matter scenario and may help to discriminate among the different possibilities in Tab. II.

Acknowledgements

We are grateful to the anonymous referee for helpful comments. The work of AI and DT was partially supported by the DFG cluster of excellence "Origin and Structure of the Universe."

---

[1] O. Adriani *et al.*, (2008), 0810.4995.

[2] I. V. Moskalenko and A. W. Strong, Astrophys. J. **493**, 694 (1998), astro-ph/9710124.

[3] S. W. Barwick *et al.* [HEAT Collaboration], Astrophys. J. **482** (1997) L191, arXiv:astro-ph/9703192.

[4] M. Boezio *et al.* [CAPRICE Collaboration], Astrophys. J. **532** (2000) 653.

[5] AMS-01, M. Aguilar *et al.*, Phys. Lett. **B646**, 145 (2007), astro-ph/0703154.

[6] J. Chang *et al.*, Nature (London) **456**, 362 (2008).

[7] S. Torii *et al.* [PPB-BETS Collaboration], arXiv:0809.0760 [astro-ph].

[8] F. Aharonian *et al.* [H.E.S.S. Collaboration], Phys. Rev. Lett. **101** (2008) 261104, arXiv:0811.3894 [astro-ph]

[9] A. K. Harding and R. Ramaty, Proc. 20th ICRC, Moscow **2**, 92-95 (1987); A. M. Atoian, F. A. Aharonian and H. J. Volk, Phys. Rev. D **52** (1995) 3265; X. Chi, E. C. M. Young and K. S. Cheng, Astrophys. J. **459** (1995) L83.

[10] D. Hooper, P. Blasi and P. D. Serpico, arXiv:0810.1527 [astro-ph].

[11] C. Grimani, Astron. Astrophys. **418**, 649 (2004)

[12] P. Blasi, arXiv:0903.2794 [astro-ph.HE]

[13] O. Adriani *et al.*, Phys. Rev. Lett. **102** (2009) 051101.

[14] H. Matsunaga *et al.*, Phys. Rev. Lett. **81** (1998) 4052.

[15] S. Orito *et al.* [BESS Collaboration], Phys. Rev. Lett. **84** (2000) 1078.

[16] M. Boezio *et al.* [WIZARD Collaboration], Astrophys. J. **487** (1997) 415.

[17] M. Boezio *et al.* [WiZard/CAPRICE Collaboration], Astrophys. J. **561** (2001) 787.

[18] J. W. Mitchell *et al.*, Phys. Rev. Lett. **76** (1996) 3057.

[19] L. Bergstrom, J. Edsjo and P. Ullio, Astrophys. J. **526** (1999) 215.

[20] F. Donato, D. Maurin, P. Salati, A. Barrau, G. Boudoul and R. Taillet, Astrophys. J. **563** (2001) 172.

[21] M. Cirelli, M. Kadastik, M. Raidal and A. Strumia, Nucl. Phys. B **813** (2009) 1, arXiv:0809.2409 [hep-ph].

[22] G. Bertone, M. Cirelli, A. Strumia and M. Taoso, JCAP **0903** (2009) 009, arXiv:0811.3744 [astro-ph].

[23] A. Ibarra and D. Tran, JCAP **0902**, 021 (2009), arXiv:0811.1555 [hep-ph].

[24] E. Nardi, F. Sannino and A. Strumia, JCAP **0901** (2009) 043, arXiv:0811.4153 [hep-ph].

[25] A. Ibarra and D. Tran, JCAP **0807**, 002 (2008), arXiv:0804.4596 [astro-ph].

[26] G. Bertone, W. Buchmuller, L. Covi and A. Ibarra, JCAP **0711** (2007) 003, arXiv:0709.2299 [astro-ph]; A. Ibarra, D. Tran and C. Weniger, arXiv:0909.3514 [hep-ph].

[27] A. Ibarra and D. Tran, Phys. Rev. Lett. **100** (2008) 061301, JCAP **0906** (2009) 004; K. Ishiwata, S. Matsumoto, and T. Moroi, Phys. Rev. **D78**, 063505 (2008), Phys. Lett. B **675**, 446 (2009); L. Covi, M. Grefe, A. Ibarra and D. Tran, JCAP **0901** (2009) 029; C.-R. Chen, F. Takahashi, and T. T. Yanagida, Phys. Lett. **B671**, 71 (2009); C.-R. Chen and F. Takahashi, JCAP **0902**, 004 (2009); P.-f. Yin *et al.*, Phys. Rev. **D79**, 023512 (2009);

K. Hamaguchi, S. Shirai, and T. T. Yanagida, Phys. Lett. B **673**, 247 (2009); M. Pospelov and M. Trott, JHEP **0904**, 044 (2009); A. Arvanitaki *et al.* arXiv:0812.2075 [hep-ph], arXiv:0904.2789 [hep-ph]; K. J. Bae and B. Kyae, JHEP **0905** (2009) 102; K. Cheung, P. Y. Tseng and T. C. Yuan, arXiv:0902.4035 [hep-ph]; S. L. Chen, R. N. Mohapatra, S. Nussinov and Y. Zhang, arXiv:0903.2562 [hep-ph]; J. Hisano, K. Nakayama and M. J. S. Yang, arXiv:0905.2075 [hep-ph]; H. Fukuoka, J. Kubo and D. Suematsu, arXiv:0905.2847 [hep-ph].

[28] A. Ibarra, A. Ringwald and C. Weniger, JCAP **0901** (2009) 003, A. Ibarra, A. Ringwald, D. Tran and C. Weniger, arXiv:0903.3625 [hep-ph]; S. Shirai, F. Takahashi and T. T. Yanagida, arXiv:0902.4770 [hep-ph].

[29] A. A. Abdo *et al.* [The Fermi LAT Collaboration], arXiv:0905.0025 [astro-ph.HE].

[30] F. Aharonian *et al.* [H.E.S.S. Collaboration] arXiv:0905.0105 [astro-ph.HE].

[31] D. Grasso *et al.* [FERMI-LAT Collaboration], arXiv:0905.0636 [astro-ph.HE].

[32] P. Meade, M. Papucci, A. Strumia and T. Volansky, arXiv:0905.0480 [hep-ph].

[33] S. Shirai, F. Takahashi and T. T. Yanagida, arXiv:0905.0388 [hep-ph]; C. H. Chen, C. Q. Geng and D. V. Zhuridov, arXiv:0905.0652 [hep-ph]; J. Mardon, Y. Nomura and J. Thaler, arXiv:0905.3749 [hep-ph]; W. Buchmuller *et al.*, arXiv:0906.1187 [hep-ph].

[34] J. F. Navarro, C. S. Frenk, and S. D. M. White, Astrophys. J. **462**, 563 (1996), astro-ph/9508025.

[35] See for example V. S. Berezinskii, S. V. Buolanov, V. A. Dogiel, V. L. Ginzburg, V. S. Ptuskin, Astrophysics of Cosmic Rays (Amsterdam: North–Holland, 1990).

[36] D. Maurin, F. Donato, R. Taillet, and P. Salati, Astrophys. J. **555**, 585 (2001), astro-ph/0101231; F. Donato, N. Fornengo, D. Maurin and P. Salati, Phys. Rev. D **69** (2004) 063501 [arXiv:astro-ph/0306207].

[37] L. J. Gleeson and W. I. Axford, Astrophys. J. **149** (1967) L115; Astrophys. J. **154** (1968) 1011.

[38] J. S. Perko, Astron. Astrophys. **184** (1987) 119.

[39] K. Ishiwata, S. Matsumoto and T. Moroi, Phys. Rev. D **79** (2009) 043527, arXiv:0811.4492 [astro-ph]; J. Zhang *et al.* arXiv:0812.0522 [astro-ph]; L. Zhang, G. Sigl and J. Redondo, arXiv:0905.4952 [astro-ph.GA].

[40] M. Cirelli and P. Panci, arXiv:0904.3830 [astro-ph.CO].

[41] K. Ishiwata, S. Matsumoto and T. Moroi, arXiv:0905.4593 [astro-ph.CO].

[42] G. R. Blumenthal and R. J. Gould, Rev. Mod. Phys. **42**, 237 (1970).

[43] T. A. Porter and A. W. Strong, arXiv:astro-ph/0507119.

[44] P. Sreekumar *et al.* [EGRET Collaboration], Astrophys. J. **494** (1998) 523.

[45] A. W. Strong, I. V. Moskalenko and O. Reimer, Astrophys. J. **613**, 956 (2004); Astrophys. J. **613** (2004) 962.

[46] T. Sjostrand, S. Mrenna, and P. Skands, JHEP **05**, 026 (2006), hep-ph/0603175.

[47] T. Bringmann and P. Salati, Phys. Rev. D **75**, 083006 (2007) [arXiv:astro-ph/0612514].

[48] A. M. Lionetto, A. Morselli and V. Zdravkovic, JCAP **0509**, 010 (2005) [arXiv:astro-ph/0502406].

[49] R. Catena and P. Ullio, arXiv:0907.0018 [astro-ph.CO].